



Enhancing phosphate adsorption by novel calcium-silicate composites: batch and column studies

Dan Jiang^{a,*}, Yoshimasa Amano^{a,b}, Motoi Machida^{a,b}

^aGraduate School of Engineering, Chiba University, 1-33 Yayoi-cho, Inage-ku, Chiba 263-8522, Japan,

emails: jiangdan1220@chiba-u.jp (D. Jiang), Amanoy@faculty.chiba-u.jp (Y. Amano), machida@faculty.chiba-u.jp (M. Machida)

^bSafety and Health Organization, Chiba University, 1-33 Yayoi-cho, Inage-ku, Chiba 263-8522, Japan

Received 23 August 2018; Accepted 8 April 2019

ABSTRACT

This paper presents two new kinds of calcium-silicate composites adsorbents KMnO_4 modified alkali-treated calcium silicate composite (KASC and Fe_3O_4 @KASC) to investigate adsorption capacity of adsorbing phosphate. The synthesized adsorbents were studied systematically by X-ray fluorescence analysis, nitrogen absorption-adsorption analyzer, X-ray diffraction, zeta potential analyzer, scanning electron microscopy and Fourier-transform infrared spectroscopy (FTIR) spectrophotometer. Factors affecting phosphate adsorption including kinetics, isotherm, pH, coexistent anions, and adsorbent dosage were investigated in batch experiments. The adsorption processes were best described by pseudo-second-order and Langmuir model, and the amount of adsorbed phosphate calculated using Langmuir model was 182 mg g^{-1} for KASC and 145 mg g^{-1} for Fe_3O_4 @KASC. Besides, Fe_3O_4 @KASC also contained magnetic property. Adsorption of phosphate by KASC and Fe_3O_4 @KASC were also performed by fixed-bed column experiments and the results were well described by Yoon-Nelson model and Thomas model. Almost all the adsorbed phosphorus could be recovered by 2% citric acid solution. The phosphate fractionation and FTIR spectra analysis indicated that $(\text{CaO})_2\text{PO}_2$ was generated during the phosphate adsorption process.

Keywords: Phosphate adsorption; Calcium-silicate composites; Batch adsorption; Column adsorption; FTIR analysis

1. Introduction

Excessive phosphorous leads to the eutrophication problem in water bodies, which causes algal blooms [1,2], impairs ecosystem balance [3] and even generates toxic materials [4] such as microcystin that may pose a threat for human health [5]. On the other hand, phosphorous is an essential element for the growth of all the organisms in the ecosystem. Nowadays most phosphorous is derived from phosphate rock, which is a non-renewable resource and current global reserves may be consumed in 50–100 years [6,7]. Therefore, it is imperative to investigate a phosphorous removed method which could also utilize the wasted phosphorous as a nutrient source. Even though there are many methods to remove phosphate from water bodies,

such as precipitation [8], wetlands system treatment [9], and membrane technology [10], adsorption is the most desirable method which can remove phosphate from water and reused for crop growing [11–13].

In our previous research, the alkali-treated calcium silicate composite (ASC) was prepared by using wasted glass and shell [14]. The effects of various parameters on phosphate adsorption were investigated in detail. ASC could remove phosphate from water with phosphate adsorption capacity of 120 mg g^{-1} , but the adsorbent saturated with phosphate after adsorption process was difficult to achieve solid-liquid separation. In order to overcome that weakness, as well as increasing the phosphate adsorption capacity, novel adsorbents should be developed to fulfil the above requirement.

* Corresponding author.

KMnO₄ can be used to modify adsorbents because of its high oxidizability, which can oxidize metal ions to their maximum valency to increase the activity of the adsorbents [15–17]. Therefore, in this study, KMnO₄ was used to treat ASC to gain a novel adsorbent named KMnO₄ modified alkali-treated calcium silicate composite (KASC) (KMnO₄-ASC). To implement the solid-liquid separation after adsorption reaction, magnetic technology is a desirable method in terms of ease of design, the simplicity of operation and low cost [18]. A magnetic adsorbent not only has a good adsorption capacity but also can be collected by a magnetic separation technology [19]. For this purpose, Fe₃O₄ was used as a magnetic carrier for preparing magnetic adsorbent due to its low cost and magnetic property.

The aim of the present study was to develop efficient adsorbents with high adsorption capacity and magnetic behavior, for removing phosphate from water. For this purpose, KASC was prepared by ASCs with KMnO₄ solution, Fe₃O₄@KASC was prepared by KASC with Fe₃O₄. Both KASC and Fe₃O₄@KASC were investigated for their potential as adsorbents to remove phosphate through batch and column experiments.

2. Materials and methods

2.1. Materials

All chemicals used in this study were of analytical reagent grade. The phosphate solution was prepared by dipotassium hydrogen orthophosphate, and all the solutions were prepared by using pure water.

The ASC was synthesized by using calcium-silicate composites (CSC) from Murakami Corporation (Chiba, Japan). 10 g of CSC were added into 50 mL of 2 M NaOH solution and the mixture was heated at 98°C by a refluxing system for 24 h. After washing several times with pure water and dehydrated ethanol, ASC was obtained [14]. The KASC was prepared by mixing 5 g ASC and 200 mL of 0.1 M KMnO₄ solution for 24 h under the room temperature. After washing several times with pure water, the KASC was obtained.

Fe₃O₄ was prepared by precipitation and partial oxidation of Fe(II) ion. 2.5 M NaOH solution was added dropwise into 0.0651 M FeSO₄ solution under high stirring speed until pH 11. After stirring for 10 min and boiling the solution in the water bath for 75 min, black liquid material was obtained. The Fe₃O₄ was obtained after washing several times with pure water and dehydrated ethanol and then dried in an oven overnight [20,21]. The Fe₃O₄@KASC was prepared by mixing 3 g KASC and 1 g Fe₃O₄ in 100 mL pure water with a strong stirring at 35°C in the water bath. After stirring for 2 h, the obtained product was washed several times with pure water and anhydrous ethanol and then dried in an oven overnight. The Fe₃O₄@KASC could be collected by the magnetic field and its magnetic property could be used in the phosphate adsorption process.

2.2. Adsorbent characterization

The elemental composition of KASC and Fe₃O₄@KASC was measured by X-ray fluorescence analysis (XRF) (RIX 2100, RIGAKU, Japan). Specific surface area and total pore volume of samples were measured by nitrogen absorption-adsorption

analyzer. (BELSORP-MINI II, MICROTRACBEL, Japan). X-ray diffraction (XRD) analysis was used to determine the crystallographic structure of samples (XRD-6100, SHIMADZU, Japan). The surface charge of adsorbents was measured by zeta potential analyzer (ZC-3000, MICROTREC, Japan). The morphological properties of samples were characterized using a scanning electron microscope (JSM-6510, JEOL, Japan). Fourier-transform infrared spectroscopy (FTIR) spectrophotometer was carried out to analyze the infrared spectra of samples before and after phosphate adsorption (IRAffinity-1, SHIMADZU, Japan). All pH values in this study were measured by pH meter (D-51, HORIBA, Japan).

2.3. Batch adsorption

Batch experiments were carried out to investigate the performance of KASC and Fe₃O₄@KASC as phosphate removal adsorbents. All the batch experiments were shaken at 100 rpm and 25°C. After specific adsorption time, the supernatant was taken to measure phosphate concentration by molybdenum-blue ascorbic method using UV-spectrophotometer (UV-2550, SHIMADZU, Japan). For the KASC adsorbent, the supernatant of phosphate solution was taken after centrifuging at 5,000 rpm for 10 min. For the Fe₃O₄@KASC adsorbent, the supernatant was taken by magnetic field to implement solid-liquid separation. The amount of adsorbed phosphate per unit mass of adsorbent (Q_e) was calculated by Eq. (1):

$$Q_e = (C_0 - C_e) \times \frac{V}{m} \quad (1)$$

where C_0 and C_e are the initial and equilibrium phosphate concentrations in mg L⁻¹, V is the volume of adsorption solution in L, m is the dry mass of adsorbent in g.

The kinetic phosphate adsorption experiments were conducted by mixing 0.6 g adsorbents in 300 mL of 500 mg L⁻¹ phosphate solution. After each specific time (0–92 h), the supernatant was taken to measure the phosphate concentration. The kinetic experimental data were fitted to pseudo-first-order and pseudo-second-order models in Eqs. (2) and (3), respectively.

$$\ln(q_e - q_t) = \ln q_e - k_1 t \quad (2)$$

$$\frac{t}{q_t} = \frac{1}{(k_2 q_e^2)} + \frac{t}{q_e} \quad (3)$$

where the q_t and q_e are the amounts of adsorbed phosphate at time t and equilibrium in mg g⁻¹. k_1 and k_2 are the adsorption rate constants in 1/h and g mg⁻¹ h⁻¹, respectively.

The isotherm phosphate adsorption experiments were conducted by mixing 0.1 g adsorbents and 50 mL phosphate solution with phosphate concentration from 20 to 600 mg L⁻¹. After shaking for 80 h, the supernatant was taken to measure the phosphate concentration and the isotherm data was fitted to Langmuir isotherm model and Freundlich isotherm model in Eqs. (4) and (5); respectively.

$$\frac{C_e}{Q_e} = \frac{C_e}{X_m} + \frac{1}{X_m K_1} \quad (4)$$

$$Q_e = K_2 C_e^{1/n} \quad (5)$$

where C_e is the phosphate concentration at equilibrium in mg L^{-1} ; Q_e is the amount of adsorbed phosphate at equilibrium in mg g^{-1} ; X_m is the maximum adsorption capacity calculated by Langmuir model in mg g^{-1} ; K_1 is the Langmuir adsorption constant in L mg^{-1} ; K_2 and n are the Freundlich adsorption constant.

To investigate the effect of solution pH on phosphate adsorption, the experiment was conducted by adding 0.1 g adsorbents into 50 mL of 500 mg L^{-1} phosphate solution with different pH range (2.0–12.0). The initial pH of the phosphate solution was adjusted by using 0.1 M HCl and 0.1 M NaOH. The supernatant was taken to measure the phosphate concentration after 80 h, and the equilibrium pH of solution (pH_e) was also measured. The effect of other anions on the phosphate adsorption was also examined by adding different adsorbent dosage (0.2–2.0 g L^{-1}) in 50 mL of 1 mmol L^{-1} phosphate solution with and without other anions (SO_4^{2-} , Cl^- , HCO_3^- , NO_3^-). After 80 h, the supernatant was taken to measure the phosphate concentration. In order to demonstrate further the performance of adsorbents for phosphate removal in the presence of natural ions, sample solution from Lake Senba (Ibaraki, Japan) was taken and then filtered through 0.45 μm membrane to remove suspended materials. A certain amount of phosphate was added into the sample solution to adjust the initial phosphate concentration to 9.97 mg L^{-1} . Various dosages (0–0.25 g L^{-1}) of adsorbents were added into 100 mL of pre-treated sample solution. After 80 h, the supernatant was taken to measure the concentration of phosphate.

2.4. Column experiments

Fixed-bed columns used in this study were made up of 0.77 μm internal diameter glass tubes and 1 g adsorbents were packed in the column to yield a bed height of 3.5 and 3.0 cm for KASC and $\text{Fe}_3\text{O}_4\text{@KASC}$, respectively. Pure water was pumped to pass the fixed-bed columns at the first 12 h to remove air bubbles and interfering substance, then the phosphate solution (10.02 mg L^{-1} , pH 7.40) was pumped downward through the column at a flow rate of 30 mL h^{-1} at the room temperature. The effluents of the column system were collected at regular time intervals and the phosphate concentrations and pH were measured. The column experimental data was fitted using Yoon and Nelson model in Eq. (6) and Thomas model in Eq. (7).

$$\ln \left[\frac{C_i}{C_i - C_t} \right] = K_{\text{YN}} (t - \theta) \quad (6)$$

where C_i and C_t are the phosphate concentrations of influent and at the time t of effluent in mg L^{-1} , K_{YN} is a adsorption constant in $1/\text{h}$ and θ is the time in h when C_t is half of C_i .

$$\frac{C_t}{C_0} = \frac{1}{1 + \exp \left(\frac{k_{\text{TH}} q_0 x}{v - k_{\text{TH}} C_0 t} \right)} \quad (7)$$

where C_0 and C_t are the phosphate concentrations of influent and effluent at time t in mg mL^{-1} , respectively; k_{TH} is the Thomas rate constant in $\text{mL min}^{-1} \text{mg}^{-1}$; q_0 is the amount of adsorbed phosphate in mg g^{-1} ; x is the mass of adsorbent in g; v is flow rate in mL min^{-1} .

The contact time of fixed-bed adsorbent and phosphate solution (T_c) was calculated by the following equation:

$$T_c = \frac{V}{v} \quad (8)$$

where V is the volume of adsorbent bed in cm^3 ; v is the flow rate of phosphate solution in mL min^{-1} .

2.5. Phosphate desorption

The KASC and $\text{Fe}_3\text{O}_4\text{@KASC}$ were initially reacted with the phosphate solution at a phosphate concentration of 500 mg L^{-1} for 80 h. After washed several times with pure water, the pre-treated adsorbents were desorbed by 2% citric acid with the liquid/solid ratio of 100 mL g^{-1} at 25°C. After 2 h, the percentage of desorbed phosphate to adsorbed phosphate was calculated to assess the possibility of recovering adsorbed phosphate.

2.6. Phosphate fractionation

The adsorbed phosphate has four different forms of phosphorus which include loosely bound-phosphorous (LB-P), alkali-soluble phosphorous (NaOH-P), acidic-soluble phosphorous (HCl-P) and residual phosphorous (Residual-P) [22]. In order to measure the concentration of different forms of phosphorous, the adsorbents were initially adsorbed phosphate at a phosphate concentration of 500 mg L^{-1} for 80 h. After washing several times by pure water, the adsorbents with adsorbed phosphate were obtained. The phosphate fractionation experiment was conducted by following steps: (1) pre-treated adsorbents were washed twice with 1 mol L^{-1} NH_4Cl solution at pH 7 for 2 h, and the desorption phosphorous was LB-P; (2) the adsorbents after treating by step 1 was washed with 0.1 mol L^{-1} NaOH solution for 16 h and the extracted phosphorous was NaOH-P; (3) the adsorbents after treated by step 2 was washed with 0.5 mol L^{-1} HCl solution twice for 2 h and the desorbed phosphorous was HCl-P; and (4) after treated by step 3, the phosphorous which still remained in adsorbents was Residual-P.

3. Results and discussion

3.1. Materials and characterization

The physicochemical properties of KASC and $\text{Fe}_3\text{O}_4\text{@KASC}$ are shown in Table 1. The main elements of KASC were O, Ca and Si with 31.0%, 26.2%, and 23.2% respectively. The main elements of $\text{Fe}_3\text{O}_4\text{@KASC}$ were Fe, O, Ca, and Si with the mass percent of 29.5%, 24.6%, 18.6%, and 16.9%, respectively. A large amount of Fe in $\text{Fe}_3\text{O}_4\text{@KASC}$ also indicated the success of composite between Fe_3O_4 and KASC. Table 1 shows that the specific surface area and average pore diameter were 139 $\text{m}^2 \text{g}^{-1}$ and 9.85 nm for KASC and

Table 1
Chemical compositions and physiochemical properties of adsorbents

Parameters	KASC	Fe ₃ O ₄ @KASC
O (%)	31.0	24.6
Fe (%)	1.12	29.5
Ca (%)	26.2	18.6
Si (%)	23.2	16.9
C (%)	7.34	4.40
Na (%)	1.14	0.71
Al (%)	1.82	1.36
K (%)	7.74	3.35
S (%)	0.05	0.13
Total (%)	99.6	99.6
BET surface area (m ² g ⁻¹)	139	112
Total pore volume (cm ³ g ⁻¹)	0.34	0.33
Pore diameter (nm)	9.85	11.9
pH value	9.60	8.90

112 m² g⁻¹ and 11.9 nm for Fe₃O₄@KASC. Both adsorbents exhibited alkaline properties with pH value of 9.80 for KASC and 8.90 for Fe₃O₄@KASC.

The XRD patterns of Fe₃O₄@KASC, KASC and Fe₃O₄ are shown in Fig. 1. Fe₃O₄ was well crystallized and it can be indexed as pure Fe₃O₄ because of the appearance of diffraction peaks at 2 theta of 30.1°, 35.5°, 37.2°, 43.2°, 57.0°, and 62.7° [23]. The KASC was shown as an amorphous structure. Meanwhile, since the diffraction peaks of Fe₃O₄@KASC were from the peaks of KASC and Fe₃O₄, there was no chemical reaction during the process of preparing Fe₃O₄@KASC. The surface charge measured as zeta potential is presented in Fig. 2 for Fe₃O₄@KASC, KASC and Fe₃O₄. The isoelectric point (IEP) of Fe₃O₄ was around 6.0, which is in agreement with other studies [24,25]. The KASC showed the IEP of 2.2, and this maybe owing to a large amount of SiO₂ with a very low IEP [25]. The IEP for Fe₃O₄@KASC was near 5.0, indicating that the surface of Fe₃O₄@KASC had positive charge when the pH was lower than 5.0. The morphology of KASC and Fe₃O₄@KASC characterized by scanning electron microscopy (SEM) are shown in Fig. 3. The KASC exhibited a rough and porous surface, which is consistent with the Brunauer–Emmett–Teller (BET) analysis. It is obviously found that the Fe₃O₄@KASC have some particle inserted into the calcium-silicate matrix. This further proved that the Fe₃O₄ particles combining with KASC and developed the magnetic adsorbent.

3.2. Adsorption kinetics

The phosphate adsorption process as a function of time is shown in Fig. 4. The results showed that the amount of adsorbed phosphate increased with increasing adsorption time and reached equilibrium at 80 h for KASC and 72 h for Fe₃O₄@KASC. Both samples adsorbed phosphate very fast in the first 24 h with the adsorbed amount of 120 and 88 mg g⁻¹ for KASC and Fe₃O₄@KASC, respectively. Then the phosphate adsorption rate became much slower and

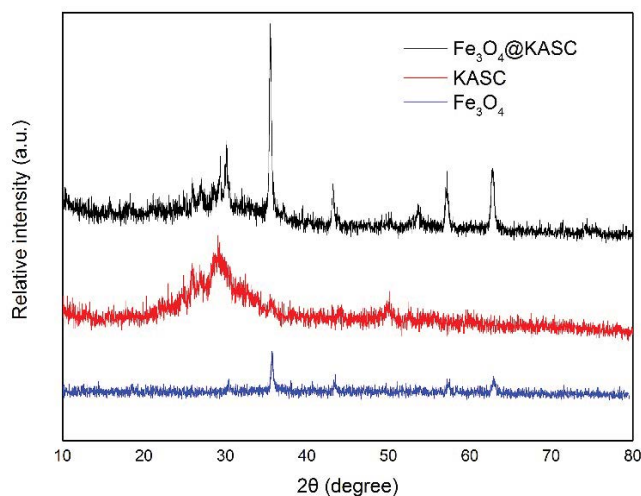


Fig. 1. XRD patterns of Fe₃O₄@KASC, KASC and Fe₃O₄.

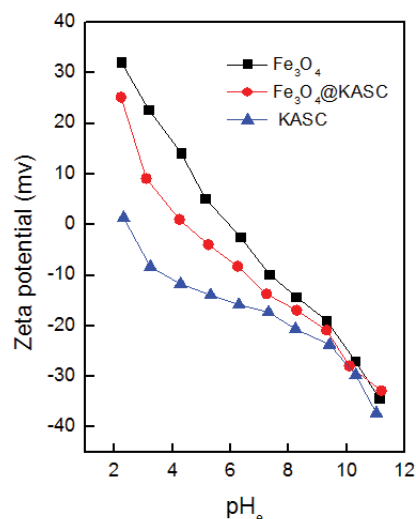


Fig. 2. Zeta potential of Fe₃O₄@KASC, KASC and Fe₃O₄.

stopped at the equilibrium time. The kinetic data was fitted the pseudo-first-order and pseudo-second-order model and the obtained equation parameters are listed in Table 2. The equation parameters showed both phosphate adsorption kinetic results were better fitted pseudo-second-order model, indicating the phosphate adsorption by KASC and Fe₃O₄@KASC were governed by diffusion courses.

3.3. Adsorption isotherm

The phosphate adsorption process as a function of the initial phosphate concentration is shown in Fig. 5. The results showed that the adsorbed phosphate amount increased with increasing equilibrium concentration, which also meant that the amount of adsorbed phosphate increased with increasing initial phosphate concentration. For KASC and Fe₃O₄@KASC, both can remove almost all the phosphate from pure water at the initial concentration from 20 to 250 mg L⁻¹. The removal rate gradually decreased and phosphate adsorption

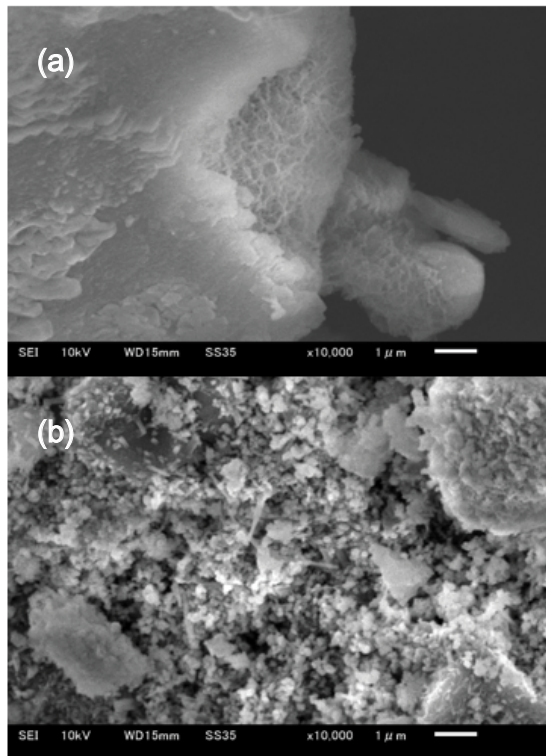


Fig. 3. The SEM of KASC (a) and Fe₃O₄@KASC (b).

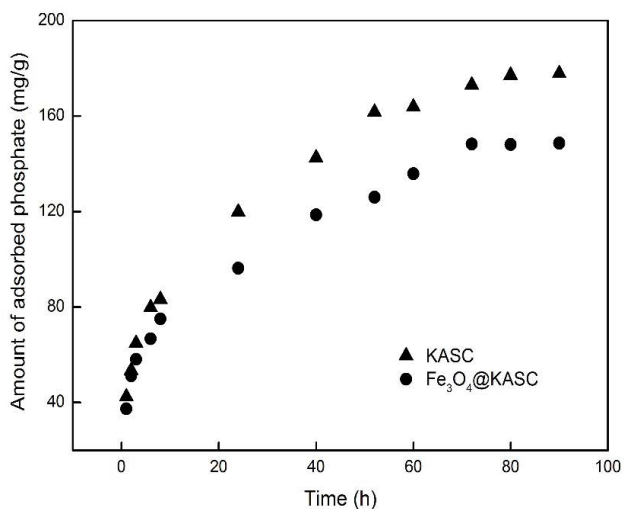


Fig. 4. The kinetic adsorption of phosphate on KASC and Fe₃O₄@KASC in pure water. (Initial phosphate concentration: 500 mg L⁻¹, adsorbent mass: 0.6 g, treated volume: 300 mL).

Table 2

Fitting parameters of the pseudo-first-order and pseudo-second-order kinetic model for the phosphate kinetic adsorption data

Adsorbents	Pseudo-first-order			Pseudo-second-order		
	q_t (mg g ⁻¹)	k_1 (1/h)	r^2	q_t (mg g ⁻¹)	k_2 (g mg ⁻¹ h ⁻¹)	r^2
KASC	190	0.06	0.883	189	6.61×10^{-4}	0.991
Fe ₃ O ₄ @KASC	153	0.06	0.885	156	8.18×10^{-4}	0.986

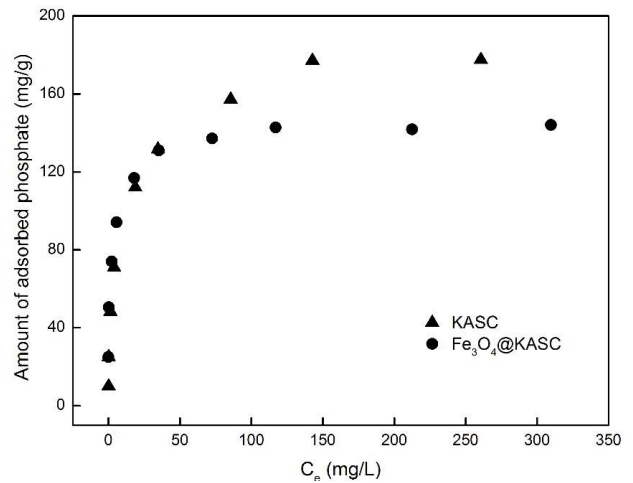


Fig. 5. The isotherm adsorption of phosphate on KASC and Fe₃O₄@KASC in pure water. (Initial phosphate concentration: 20–600 mg L⁻¹, adsorbent mass: 0.1 g, treated volume: 50 mL, contact time: 80 h).

finally stopped until the adsorption reached saturation. The isotherm data was fitted to the Langmuir and Freundlich model and the fitting parameters are listed in Table 3. The parameters showed that the isotherm adsorption results were better fitted the Langmuir equation, and the maximum adsorption capacity of KASC and Fe₃O₄@KASC calculated by Langmuir were 182 and 145 mg g⁻¹, respectively.

3.4. pH influence

The influence of initial phosphate solution pH on the phosphate adsorption by KASC and Fe₃O₄@KASC was investigated in a wide pH range from 1.90 to 12.0 and the results are shown in Fig. 6. The relationship between initial phosphate solution pH and pH_i is also shown in Table 4. Both adsorbents exhibited a good phosphate adsorption capacity over a wide pH range from 2.35 to 12.0 for KASC and from

Table 3

Fitting parameters of the Langmuir and Freundlich model for the phosphate isotherm adsorption data

Adsorbents	Langmuir model			Freundlich		
	X_m (mg g ⁻¹)	K_1 (L mg ⁻¹)	r^2	n	K_2	r^2
KASC	182	0.162	0.997	3.42	42.6	0.935
Fe ₃ O ₄ @KASC	145	0.421	0.999	6.57	68.2	0.944

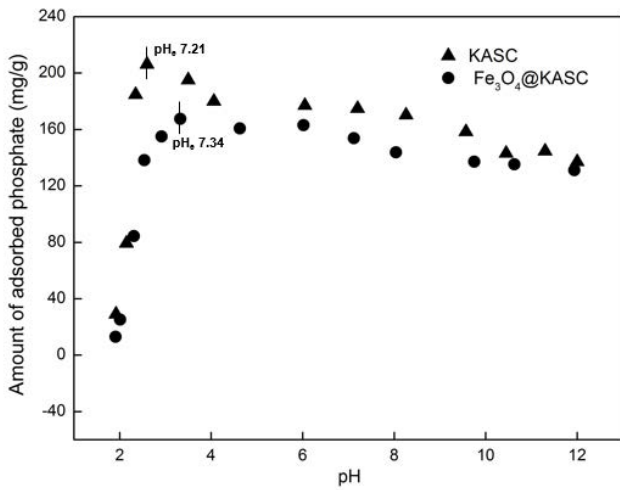
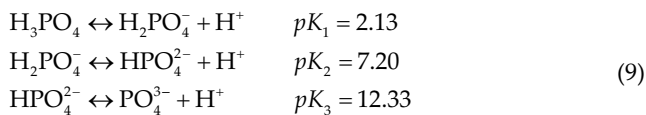


Fig. 6. The effect of initial pH value of phosphate solution on the phosphate adsorption by KASC and Fe₃O₄@KASC in pure water. (Initial phosphate concentration: 500 mg L⁻¹, adsorbent mass: 0.1 g, treated volume: 50 mL, contact time: 80 h).

2.54 to 12.0 for Fe₃O₄@KASC. For the KASC, the amount of adsorbed phosphate increased very fast with increasing initial pH range from 1.92 to 2.60 (pH_e 3.22–7.21). After that, the phosphate adsorption amount decreased slightly with the further increase of initial pH values from 2.60 to 12.0 (pH_e 7.21–11.8). For the Fe₃O₄@KASC, the amount of adsorbed phosphate increased rapidly with increasing pH value from 1.91 to 3.33 (pH_e 2.73–7.34), while the trend of adsorbed phosphate decreased slowly with increasing pH from 3.33 to 11.9 (pH_e 7.34–11.4).

pH plays a significant role in the determination of the concentration of phosphate species in the aqueous system. The relationship between pH and phosphate species was summarized in the following equation [26]:



Therefore, when pH_e moves from 2.13 to 7.20, H₂PO₄⁻ was the main species in the phosphate solution. After that, HPO₄²⁻ became the dominated species in pH_e range 7.20–12.33. Fig. 6 shows that when pH_e value was around 7.2, KASC and Fe₃O₄@KASC could adsorb highest phosphate amount of 206 and 167 mg g⁻¹, respectively. There were two reasons for this: on the one hand, the adsorption free energy of H₂PO₄⁻ was lower than that of HPO₄²⁻, so the H₂PO₄⁻ was more easily adsorbed by adsorbents [27]. On the other hand, the process of phosphate adsorption also needs the participation of OH⁻, but when the pH was higher than 7.2, the amount of OH⁻ was too much in solution which could compete with phosphate on the active adsorption sites of adsorbent, and this also explained the amount of adsorbed phosphate reduced with increasing pH_e from 7.2 to 12.0 [26,28]. Meanwhile, when pH_e increased from 7.2 to 12.0, an increasing electrostatic repulsion between adsorbents and phosphate ions also induced a lower phosphate adsorption.

3.5. Influence of coexistent anions

Most phosphate adsorption was interfered by other anions which may compete for adsorption sites. Therefore, the influence of coexisting anions on phosphate adsorption by KASC and Fe₃O₄@KASC were examined and the results are shown in Fig. 7. When the adsorbent dosage was lower than 1.0 g L⁻¹, the phosphate adsorption amount in sole phosphate solution was higher than that in anions-mixed solution for both KASC and Fe₃O₄@KASC. The adsorbent dosage was higher than 1.0 g L⁻¹ when the amount of adsorbed phosphate in sole phosphate solution and anions-mixed solution was similar. Therefore, the other anions could compete with phosphate for the adsorption sites,

Table 4
pH value of phosphate solution at initial and equilibrium time

KASC		Fe ₃ O ₄ @KASC	
Initial pH	Equilibrium pH	Initial pH	Equilibrium pH
1.92	3.22	1.91	2.73
2.15	5.83	2.01	3.17
2.35	6.64	2.31	6.02
2.60	7.21	2.54	6.31
3.50	9.51	2.92	7.19
4.06	9.73	3.33	7.34
6.05	9.80	4.63	8.13
7.20	10.1	6.02	8.53
8.26	10.2	7.12	9.73
9.57	10.3	8.04	9.95
10.4	10.7	9.75	10.1
11.3	11.4	10.6	10.2
12.0	11.8	11.9	11.4

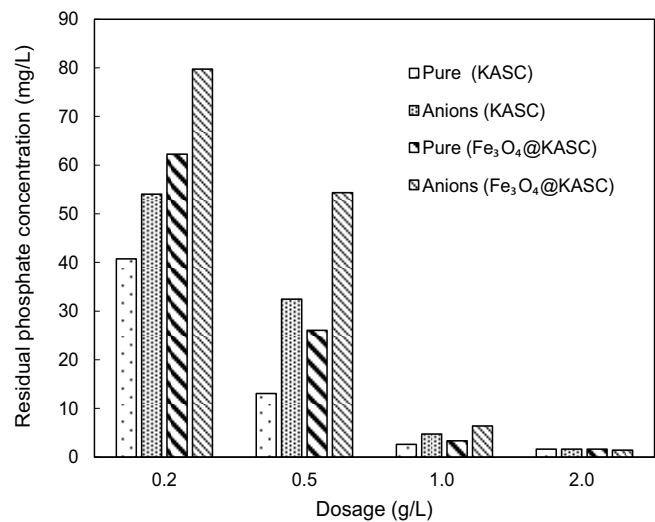


Fig. 7. Influence of coexistent anions on phosphate adsorption by KASC and Fe₃O₄@KASC in pure water. (Initial phosphate concentration: 1 mmol L⁻¹, adsorbent dosage: 0.2–2.0 g L⁻¹, treated volume: 50 mL, contact time: 80 h, coexisting anions: SO₄²⁻, Cl⁻, HCO₃⁻, NO₃⁻).

but the coexistent anions effect reduced with increasing adsorption sites.

3.6. Phosphate adsorption in natural water

The influence of adsorbent dosage on phosphate removal from natural water was studied by varying adsorbent dosage from 0.02 to 0.25 g L⁻¹ with an initial phosphate concentration of 9.97 mg L⁻¹. The increased adsorbent dosage has more adsorptive sites and a greater surface area. Therefore, as shown in Fig. 8, the removal efficiency of phosphate increased with increasing adsorbent dosage. Meanwhile, the residual phosphate concentration was decreased to 0.2 mg L⁻¹ for KASC and Fe₃O₄@KASC at the dosage of 0.20 and 0.25 g L⁻¹, respectively. Phosphate concentration of 0.2 mg L⁻¹ in lake water was satisfied with the requirement of environmental quality standard for lakes in Japan (0.3 mg PO₄³⁻ L⁻¹). Hence, for the future industrial utilization, to treat 10 m³ of waste water containing 10 mg L⁻¹ phosphate to reach the environmental quality standard for lakes, only 2 kg of KASC and 2.5 kg of Fe₃O₄@KASC is required.

3.7. Column adsorption

The breakthrough curves of phosphate on KASC and Fe₃O₄@KASC column are shown in Fig. 9. For the KASC, the breakthrough and exhausting point was around 4,100 and 9,600 mL, respectively. For the Fe₃O₄@KASC, the breakthrough and exhausting point was around 4,300 and 10,500 mL, respectively. Both column adsorption data was fitted to the Yoon and Nelson model and Thomas model, and the obtained parameters are listed in Table 5. For the Yoon and Nelson equation, the θ values calculated by Eq. (6) were similar with that obtained from experimental data, implying both column adsorption results had a good agreement with Yoon and Nelson model [29]. After calculation with Thomas model, the saturation adsorption amount was 77.1 mg g⁻¹ for KASC and 80.3 mg g⁻¹ for Fe₃O₄@KASC, which was

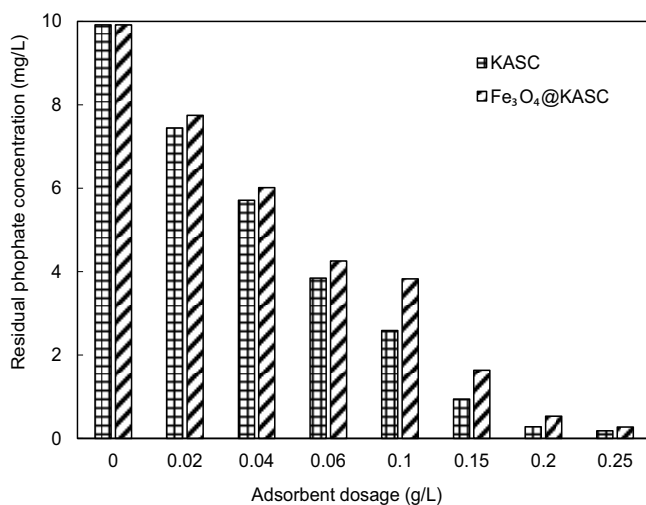


Fig. 8. The adsorption of phosphate on KASC and Fe₃O₄@KASC as a function of adsorbent dosage in natural water. (Initial phosphate concentration: 9.97 g L⁻¹, treated volume: 100 mL, contact time: 80 h).

much lower than that obtained from batch experiments with 182 and 145 mg g⁻¹, respectively. There were two reasons: firstly, the initial concentration of phosphate in the column experiment was much lower than that of batch experiment; secondly, the condition of column adsorption and batch adsorption were different, and column adsorption always treats fresh phosphate solution before reaching adsorption equilibrium. In this study, the contact time between adsorbents and phosphate was 2.8 min for KASC and 3.3 min for Fe₃O₄@KASC, so the limited contact time between phosphate solution and adsorbent decreased the phosphate adsorption capacity. Even the amount of adsorbed phosphate by column adsorption was much lower than that of batch adsorption, there was no doubt that fixed-bed system was much more popularly utilized in real wastewater treatment because of simply, continuously and economically operation [30].

3.8. Phosphate desorption

The phosphorous content in KASC and Fe₃O₄@KASC after adsorbing phosphate is high. However, the adsorbed phosphorous cannot directly desorb into water because the

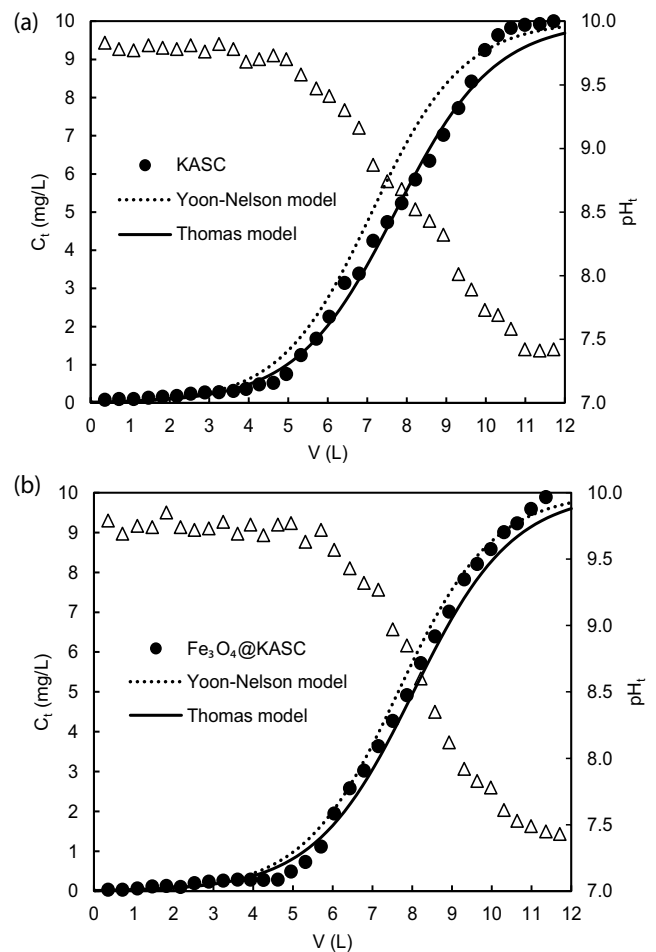


Fig. 9. Breakthrough curve of phosphate adsorption on (a) KASC and (b) Fe₃O₄@KASC column. Solid circle: C_1 , open triangle: pH_1 . (Initial phosphate concentration: 10.02 mg L⁻¹, adsorbent mass: 1 g, flow rate: 30 mL h⁻¹).

Table 5
Fitting parameters of the Noon and Nelson model and Thomas model for the phosphate isotherm adsorption data

Adsorbents	Yoon and Nelson model				Thomas model		
	K_{YN} (h^{-1})	θ_{cal} (h)	θ_{exp} (h)	r^2	k_{TH} ($mL\ min^{-1}\ mg^{-1}$)	q_0 ($mg\ g^{-1}$)	r^2
KASC	0.026	238	251	0.952	0.04	77.1	0.952
$Fe_3O_4@KASC$	0.025	255	263	0.941	0.04	80.3	0.941

generated phosphorous complex is insoluble. The Japanese Fertilizer of Control Act defines the citrate solubility (soluble in 2% citric acid solution) as a criterion. In other words, if phosphorous complex can be desorbed by 2% citric acid solution, the phosphorous can be released into natural soil and used as fertilizer. Table 6 showed that the desorption ratio of adsorbed phosphorous was 95.6% for KASC and 97.5% for $Fe_3O_4@KASC$. The results indicate that the adsorbents saturated with phosphorus can be directly released into soil. In this study, the adsorbents contain a large proportion of calcium, and the calcium element can also be used for agriculture as Ca ions is a necessary nutrient for crop growth. The citric acid is widely known for dissolving calcium compounds, and Table 6 showed that the second phosphate adsorption amount is very low, so most of Ca ions released into citric acid. Therefore, the KASC and $Fe_3O_4@KASC$ after adsorbed phosphate are promising phosphate and calcium fertilizer for crop growth.

3.9. Adsorption mechanism

As the XRF analysis, the main element of KASC and $Fe_3O_4@KASC$ was O, Ca, Si and O, Fe, Ca, Si, respectively. Therefore, those elements were the main effect on adsorbing phosphate. To illustrate phosphate adsorption mechanism, the phosphate fractionation experiment was conducted and the results are given in Table 7. The results showed that approximately 93.9% and 91.3% adsorbed phosphate was recovered by HCl solution, indicating that the main adsorbed phosphate was HCl-P. As the adsorbed phosphate cannot be desorbed by NaOH, but can be desorbed by HCl, that means the Ca-P or Mg-P was generated [22]. Therefore, in this study, calcium-phosphate composites were generated on

the surface of KASC and $Fe_3O_4@KASC$. To further elucidate phosphate adsorption mechanism, FTIR spectra was used to analysis adsorbents before and after adsorbing phosphate and the results are shown in Fig. 10. For both KASC and $Fe_3O_4@KASC$ adsorbents, after adsorbing phosphate, the FTIR band of P complex appeared at 1028 and 962 cm^{-1} , proving that the phosphate complex was generated during the process of phosphate adsorption [31–33]. The phosphate complex included $(XO)_3PO$ species with C_{3v} symmetry, $(XO)_2PO_2$ species with C_{2v} symmetry and $XOPO_3$ species with C_{3v} symmetry, where X represents the metal element or H, and each species has its special FTIR bands [31]. The bands occurring at 1,028 and 962 cm^{-1} in this study indicated

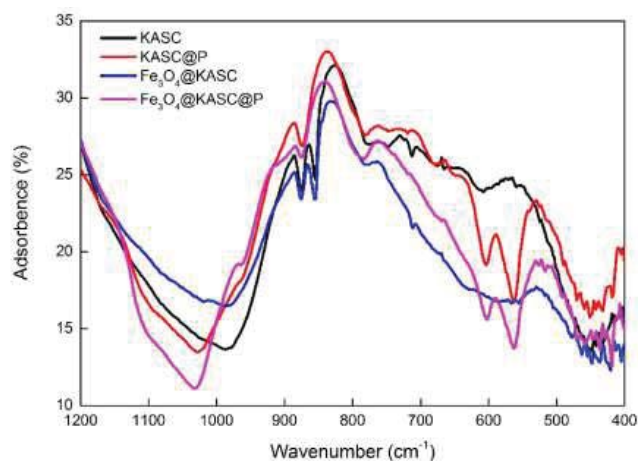


Fig. 10. The FTIR spectra of KASC and $Fe_3O_4@KASC$ before and after adsorbing phosphate.

Table 6
Desorption of adsorbed phosphate by 2% citric acid

Adsorbents	1st adsorption ($mg\ g^{-1}$)	Desorption ($mg\ g^{-1}$)	Recovery rate (%)	2nd adsorption ($mg\ g^{-1}$)
KASC	179	171	95.6	16.3
$Fe_3O_4@KASC$	136	132	97.5	21.1

Table 7
Fractionation of adsorbed phosphate

Adsorbents	LB-P		NaOH-P		HCl-P		Residual-P	
	q ($mg\ g^{-1}$)	%						
KASC	1.38	0.75	5.08	2.76	173	93.9	4.88	2.65
$Fe_3O_4@KASC$	2.46	1.54	5.96	3.73	146	91.3	5.46	3.41

that the species with C_{2v} symmetry were generated, and the two bands can be taken for ν_{as} and ν_s P–O stretching vibration bands, respectively. Therefore, the generated phosphate complex during phosphate adsorption is $(CaO)_2PO_2$ [26].

4. Conclusion

In this study, KASC and $Fe_3O_4@KASC$ adsorbents were prepared for phosphate adsorption and found to have good phosphate adsorption capacities. Using Langmuir model, the phosphate adsorption capacities of KASC and $Fe_3O_4@KASC$ were 182 and 145 mg g^{-1} , respectively. $Fe_3O_4@KASC$ not only had high phosphate adsorption capacity, but also had magnetic property to remove the pollutants from the solution by a magnetic separation technology. For KASC and $Fe_3O_4@KASC$, the phosphate adsorption processes were best described by the pseudo-second-order and Langmuir model. Both adsorbents can exhibit high phosphate adsorption capacity over a wide pH range (pH 2.30–12.0 for KASC; pH 2.54–12.0 for $Fe_3O_4@KASC$). The coexistent anions reduced the phosphate adsorption at the low adsorbent dosage, but the influence became slight when the adsorbent dosage increased. The removal of phosphate (~ 10 mg L^{-1}) from natural water by adsorbents performed well at the dosage of 2.0 kg/10 m^3 for KASC and 2.5 kg/10 m^3 for $Fe_3O_4@KASC$. In the column experiments, the breakthrough points of KASC and $Fe_3O_4@KASC$ was 4,300 and 5,300 mL, respectively. The experimental results had good agreement with Yoon and Nelson Model and Thomas Model, and the saturation adsorption amount calculated by Thomas Model was 38.5 and 41.2 mg g^{-1} for KASC and $Fe_3O_4@KASC$, respectively. The adsorbed phosphorous by adsorbents can be desorbed more than 95% by 2% citric acid solution. Through phosphate fractionation and FTIR analysis, the adsorption mechanism in this study would be due to generating $(CaO)_2PO_2$ composition during phosphate adsorption reaction.

Acknowledgments

This study was funded in part by the Japan Society for the Promotion of Science (JSPS) under Grants-in-aid for Scientific Research (C) (No. 26340058) and Grant-in-aid for Encouragement of Young Scientists (B) (No. 15K18142). The first author also acknowledges the kind support of the Japanese Government (MEXT) for the scholarship through the Super Global University Project.

References

- [1] M. Chen, S. Ding, X. Chen, Q. Sun, X. Fan, J. Lin, M. Ren, L. Yang, C. Zhang, Mechanisms driving phosphorus release during algal blooms based on hourly changes in iron and phosphorus concentrations in sediments, *Water Res.*, 133 (2018) 153–169.
- [2] D.J. Conley, H.W. Paerl, R.W. Howarth, D.F. Boesch, S.P. Seitzinger, K.E. Havens, K.E. Havens, C. Lancelot, G.E. Likens, Controlling eutrophication: nitrogen and phosphorus, *Science*, 123 (2009) 1014–1015.
- [3] X. Chuai, W. Ding, X. Chen, X. Wang, A. Miao, B. Xi, L. He, L. Yang, Phosphorus release from cyanobacterial blooms in Meiliang Bay of Lake Taihu, China, *Ecol. Eng.*, 37 (2011) 842–849.
- [4] T.W. Davis, M.J. Harke, M.A. Marcoval, J. Goleski, C. Orano-Dawson, D.L. Berry, C.J. Gobler, Effects of nitrogenous compounds and phosphorus on the growth of toxic and non-toxic strains of *Microcystis* during cyanobacterial blooms, *Aquat. Microb. Ecol.*, 61 (2010) 149–162.
- [5] D.R. de Figueiredo, U.M. Azeiteiro, S.M. Esteves, F.J.M. Gonçalves, M.J. Pereira, Microcystin-producing blooms—a serious global public health issue, *Ecotoxicol. Environ. Saf.*, 59 (2004) 151–163.
- [6] D. Cordell, J.-O. Drangert, S. White, The story of phosphorus: global food security and food for thought, *Global Environ. Change*, 19 (2009) 292–305.
- [7] D. Cordell, S. White, Peak phosphorus: clarifying the key issues of a vigorous debate about long-term phosphorus security, *Sustainability*, 3 (2011) 2027–2049.
- [8] M.K. de Kreuk, J.J. Heijnen, M.C. van Loosdrecht, Simultaneous COD, nitrogen, and phosphate removal by aerobic granular sludge, *Biotechnol. Bioeng.*, 90 (2005) 761–769.
- [9] C. Vohla, M. Köiv, H.J. Bavor, F. Chazarenc, Ü. Mander, Filter materials for phosphorus removal from wastewater in treatment wetlands—a review, *Ecol. Eng.*, 37 (2011) 70–89.
- [10] S. Yang, F. Yang, Z. Fu, T. Wang, R. Lei, Simultaneous nitrogen and phosphorus removal by a novel sequencing batch moving bed membrane bioreactor for wastewater treatment, *J. Hazard. Mater.*, 175 (2010) 551–557.
- [11] J. Xie, Y. Lin, C. Li, D. Wu, H. Kong, Removal and recovery of phosphate from water by activated aluminum oxide and lanthanum oxide, *Powder Technol.*, 269 (2015) 351–357.
- [12] Z. Ma, Q. Li, Q. Yue, B. Gao, W. Li, X. Xu, Q. Zhong, Adsorption removal of ammonium and phosphate from water by fertilizer controlled release agent prepared from wheat straw, *Chem. Eng. J.*, 171 (2011) 1209–1217.
- [13] X. Liu, L. Zhang, Removal of phosphate anions using the modified chitosan beads: adsorption kinetic, isotherm and mechanism studies, *Powder Technol.*, 277 (2015) 112–119.
- [14] D. Jiang, Y. Amano, M. Machida, Removal and recovery of phosphate from water by calcium-silicate composites-novel adsorbents made from waste glass and shells, *Environ. Sci. Pollut. Res.*, 24 (2017) 8210–8218.
- [15] Y.-H. Huang, Y.-J. Shih, F.-J. Cheng, Novel $KMnO_4$ -modified iron oxide for effective arsenite removal, *J. Hazard. Mater.*, 198 (2011) 1–6.
- [16] Q. Shi, J. Zhang, C. Zhang, W. Nie, B. Zhang, H. Zhang, Adsorption of Basic Violet 14 in aqueous solutions using $KMnO_4$ -modified activated carbon, *J. Colloid Interface Sci.*, 343 (2010) 188–193.
- [17] Y. Wang, X. Wang, X. Wang, M. Liu, L. Yang, Z. Wu, S. Xia, J. Zhao, Adsorption of Pb(II) in aqueous solutions by bamboo charcoal modified with $KMnO_4$ via microwave irradiation, *Colloids Surf., A*, 414 (2012) 1–8.
- [18] L.-g. Yan, K. Yang, R.-r. Shan, T. Yan, J. Wei, S.-j. Yu, H.-q. Yu, B. Du, Kinetic, isotherm and thermodynamic investigations of phosphate adsorption onto core-shell $Fe_3O_4@LDHs$ composites with easy magnetic separation assistance, *J. Colloid Interface Sci.*, 448 (2015) 508–516.
- [19] L. Lai, Q. Xie, L. Chi, W. Gu, D. Wu, Adsorption of phosphate from water by easily separable $Fe_3O_4@SiO_2$ core/shell magnetic nanoparticles functionalized with hydrous lanthanum oxide, *J. Colloid Interface Sci.*, 465 (2016) 76–82.
- [20] M. Yamaura, D.A. Fungaro, Synthesis and characterization of magnetic adsorbent prepared by magnetite nanoparticles and zeolite from coal fly ash, *J. Mater. Sci.*, 48 (2013) 5093–5101.
- [21] D. Jiang, Y. Amano, M. Machida, Removal and recovery of phosphate from water by a magnetic $Fe_3O_4@ASC$ adsorbent, *J. Environ. Chem. Eng.*, 5 (2017) 4229–4238.
- [22] A.H.M. Hieltsjes, L. Lijklema, Fractionation of inorganic phosphates in calcareous sediments, *J. Environ. Qual.*, 9 (1980) 405–407.
- [23] J. Qu, G. Liu, Y. Wang, R. Hong, Preparation of Fe_3O_4 -chitosan nanoparticles used for hyperthermia, *Adv. Powder Technol.*, 21 (2010) 461–467.
- [24] Y.-C. Chang, D.-H. Chen, Preparation and adsorption properties of monodisperse chitosan-bound Fe_3O_4 magnetic nanoparticles

- for removal of Cu(II) ions, *J. Colloid Interface Sci.*, 283 (2005) 446–451.
- [25] J. Wang, S. Zheng, Y. Shao, J. Liu, Z. Xu, D. Zhu, Amino-functionalized Fe₃O₄@SiO₂ core-shell magnetic nanomaterial as a novel adsorbent for aqueous heavy metals removal, *J. Colloid Interface Sci.*, 349 (2010) 293–299.
- [26] J. Xie, Z. Wang, S. Lu, D. Wu, Z. Zhang, H. Kong, Removal and recovery of phosphate from water by lanthanum hydroxide materials, *Chem. Eng. J.*, 254 (2014) 163–170.
- [27] N.I. Chubar, V.A. Kanibolotskiy, V.V. Strelko, G.G. Gallios, V.F. Samanidou, T.O. Shaposhnikova, V.G. Milgrandt, I.Z. Zhuravlev, Adsorption of phosphate ions on novel inorganic ion exchangers, *Colloids Surf., A*, 255 (2005) 55–63.
- [28] C. Fang, T. Zhang, P. Li, R.F. Jiang, Y.C. Wang, Application of magnesium modified corn biochar for phosphorus removal and recovery from swine wastewater, *Int. J. Environ. Res. Public Health*, 11 (2014) 9217–9237.
- [29] E. Zong, D. Wei, H. Wan, S. Zheng, Z. Xu, D. Zhu, Adsorptive removal of phosphate ions from aqueous solution using zirconia-functionalized graphite oxide, *Chem. Eng. J.*, 221 (2013) 193–203.
- [30] E. Malkoc, Y. Nuhoglu, Y. Abali, Cr(VI) adsorption by waste acorn of *Quercus ithaburensis* in fixed beds: prediction of breakthrough curves, *Chem. Eng. J.*, 119 (2006) 61–68.
- [31] E.J. Elzinga, D.L. Sparks, Phosphate adsorption onto hematite: an in situ ATR-FTIR investigation of the effects of pH and loading level on the mode of phosphate surface complexation, *J. Colloid Interface Sci.*, 308 (2007) 53–70.
- [32] G.I. Lampronti, G. Artioli, L. Oliva, A. Ongaro, S. Maretto, F. Bonino, K. Barbera, S. Bordiga, Role of phosphate species and speciation kinetics in detergency solutions, *Ind. Eng. Chem. Res.*, 51 (2012) 4173–4180.
- [33] C. Luengo, M. Brigante, J. Antelo, M. Avena, Kinetics of phosphate adsorption on goethite: comparing batch adsorption and ATR-IR measurements, *J. Colloid Interface Sci.*, 300 (2006) 511–518.